Hermite-Rodriguez UWB Circular Arrays

Gaetano Marrocco, *Member, IEEE*, and Giovanni Galletta

***Abstract*—Pulsed circular arrays are collecting growing interest in radar applications such as automotives and indoor navigations. This contribution presents the analytic derivation of the space-time and energy patterns of pulsed circular arrays in terms of geometrical and electrical parameters as well as of the signal distortion produced by the antennas' response. It is shown that the field emitted by circular arrays with many elements can be represented as a summation of a practically finite set of high-order Hermite-Rodriguez waveforms, while the energy pattern is a generalized Hypergeometric Function. The angular and temporal resolutions are finally related, through handy formulas, to the array size, the input signals and to the antenna types.**

***Index Terms*—Circular array, Hermite-Rodriguez functions, pulsed arrays, ultrawideband (UWB) antennas.**

I. Introduction

In the last decades there has been an increasing interest in ultrawideband (UWB) pulsed arrays [1]–[3] consisting in an arrangement of antennas having more than 25% bandwidth, which are sourced by baseband carrier-free input signals. Possible applications are for communications, radar, precise indoor positioning and tracking [4]–[6]. The properties of UWB pulses permit to design "spots" as opposed to "beams" in narrow band systems and hence a set of distributed radios can be used to communicate to a distant specific point in space.

Pulsed linear arrays (PLA) have been theoretically investigated from different points of view for what concerns the general features [7]–[12], the dynamics of ultrasparse configurations [13] and the modal phenomena arising in large, at limit infinite, two-dimensional configurations [14], [15]. Since real antennas have a finite bandwidth, they produce a distortion of the input waveform so that the radiated signals depend on both the array geometry and beamforming network as well as on the antenna space-time features. These effects can not be simply kept separate as instead commonly done in the narrowband regime. A few synthesis techniques have been moreover presented with the underlying idea to control the individual waveforms exciting each antenna with the goal to achieve localized radiation [16], [17] or the compliance with a given mask having imposed some constraints over the beamforming network [18].

Manuscript received December 01, 2008; revised September 10, 2009. First published December 04, 2009; current version published February 03, 2010.

G. Marrocco is with the Dipartimento di Informatica, Sistemi e Produzione, University of Roma "Tor Vergata", Roma, Italy (e-mail: marrocco@disp.uniroma2.it).

G. Galletta was with the Dipartimento di Informatica, Sistemi e Produzione, University of Roma "Tor Vergata", Roma, Italy. He is now with Terasystem SpA, Rome 00143, Italy (e-mail: giovanni.galletta@gmail.com).

Color versions of one or more of the figures in this paper are available online at http://ieeexplore.ieee.org.

Digital Object Identifier 10.1109/TAP.2009.2037695

Pulsed circular arrays (PCA) are particular attractive in precise radar applications such as indoor radio-navigation, automotive radars and homeland surveillance. PCA are recognized to can provide better angle of arrival estimates [19] than linear array and planar rectangular arrays, in light of the following two important advantages: i) the azimuth of PCA covers 360 ° in contrast to the 180 ° of PLAs; ii) the spot of the PCA is unchanged for scanning around the azimuth angle while that of the PLA broadens and distorts as the spot is steered from the boresight [20]. Moreover it is has been demonstrated that PCA recordings contain 3D information, which can be used to identify, separate, and reconstruct first-order ceiling reflections in indoor environments [21].

PCA configurations have been mainly studied in acoustics and optics for impulse-like input signals because of their relevance to sound and image formation. Many publications may be found about the possibility to achieve highly localized and non-diffracting waves (see the book [22] for an exhaustive review). Fewer contributions are instead available about the electromagnetic properties of PCAs. The study in [23] introduces the main formalism and gives many numerical examples for the only Gaussian input waveform with no specification of the single antenna features. The mathematical properties of pulse-driven antennas are instead considered in [16] with a particular emphasis to the formation of non diffracting beams and analytical examples for annular arrays of short dipoles are discussed with a detailed physical insight.

In this paper the UWB radiation from circular arrays is addressed for higher-order Gaussian input stimuli and for canonical models of distorting antennas within the unitary framework of Hermite Rodriguez representation of signals. A new class of pulsed circular arrays is therefore originated: the Hermite-Rodriguez arrays, and the purpose of the work is to establish some fundamental limits in beam formation and to provide handy relationships among the global radiation features and the geometrical and electrical parameters useful for a preliminary array design. In particular, analytical formulas are derived in the case of array with many elements for both the space-time radiated field and the energy pattern. The proposed representation permits, moreover, to give a simple interpretation to the formation of the transient radiated patterns in terms of superposition of Hermite-Rodriguez waveforms.

The paper is organized as follow: Section II briefly recalls the formalism of transient circular arrays and introduces the concept of ideal mth order Hermite-Rodriguez array. Section III deals with the representation and UWB properties of circular arrays with many elements by means of exact expressions. Section IV shows some examples to better understand the role of the geometrical and physical parameters and, finally, Section IV gives some preliminary considerations of further issues arising for real systems.

0018-926X/$26.00 © 2009 IEEE

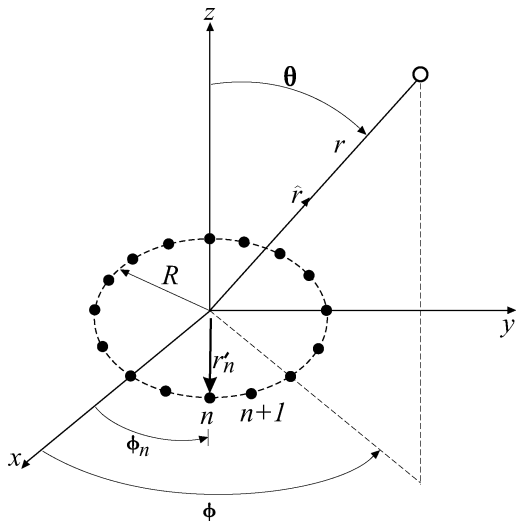

Fig. 1. Geometry and reference system of a circular array of N elements.

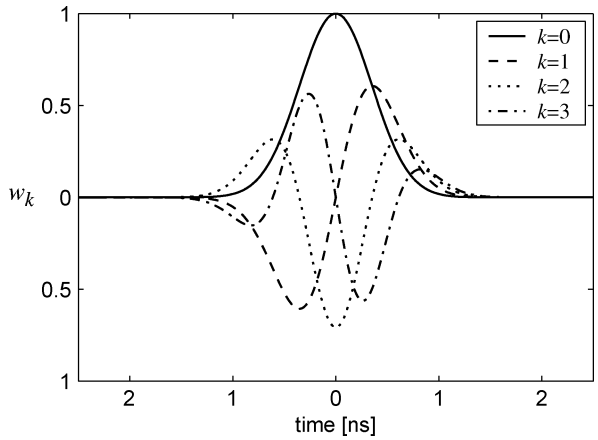

Fig. 2. Hermite-Rodriguez functions of some order k.

II. Circular Arrays in Pulsed Regime

Time-dependent radiation from antennas is generally described by the *transmitting-mode Time Domain (TD) effective height* [24] $\boldsymbol{h}^t(\hat{\boldsymbol{r}},t)$ which accounts for the antenna-source mismatch and depends on the time t and on the observation unitary vector $\hat{\boldsymbol{r}}(\theta,\phi)=[\cos\phi\sin\theta\hat{\boldsymbol{x}}+\sin\phi\sin\theta\hat{\boldsymbol{y}}+\cos\theta\hat{\boldsymbol{z}}]$.

A set of N identical and equi-oriented antennas, each excited by an inward travelling current $i_n^+(\tau)$, is now considered. Following usual far-field approximations [24], the total field radiated by the array, when the coupling effects are neglected, is

$$\boldsymbol{E}^A(\boldsymbol{r},t)=-\frac{\eta_0}{4\pi rc}\left[\boldsymbol{h}^t(\hat{\boldsymbol{r}},\cdot)*\mathcal{F}(\hat{\boldsymbol{r}},\cdot)\right]\left(t-\frac{r}{c}\right) \tag{1}$$

where c is the speed of light and η_0 the vacuum impedance. The function

$$\mathcal{F}(\hat{\boldsymbol{r}},\tau)=\sum_{n=1}^{N} i_n^+\left(\tau+t_n(\hat{\boldsymbol{r}})\right) \tag{2}$$

is the TD array factor [9] with $t_n(\hat{\boldsymbol{r}})=((\boldsymbol{r}'_n\cdot\hat{\boldsymbol{r}})/c)+t_{d,n}$. $t_{d,n}$ is a time delay to achieve spot steering along a given direction $\hat{\boldsymbol{r}}$, and $\boldsymbol{r}'_n$ tags the nth antenna position with respect to a local coordinate system.

For a circular equi-spaced array of radius R (Fig. 1) whose input currents are delayed to focus the main spot along $\hat{\boldsymbol{r}}_0=\hat{\boldsymbol{r}}(\theta_0,\phi_0)$ direction, the term, $t_n(\hat{\boldsymbol{r}})$ may be expressed, according the formalism in [23], as

$$t_n(\hat{\boldsymbol{r}})=\frac{R\left[\sin\theta\cos(\phi-\phi_n)-\sin\theta_0\cos(\phi_0-\phi_n)\right]}{c} \tag{3}$$

where $\phi_n=n\Delta\phi=2\pi n/N$ is the angular position of the arrays elements and $t_n(\hat{\boldsymbol{r}}_0)=0$.

A. Hermite-Rodriguez Arrays

Uniform arrays are here considered, in the sense that all the antennas are supposed to be sourced by the same input waveform and specific delay. In particular, such waveforms belong to the family of high-order Gaussian pulses, also known as Hermite-Rodriguez functions [25] defined as

$$w_k(t)=\frac{(-1)^k(\sqrt{2}\sigma)^k}{\sqrt{2^k k!}}\frac{d^k}{dt^k}\frac{1}{\sqrt{2\pi}\sigma}e^{-t^2/2\sigma^2} \tag{4}$$

where "k" tags the order of the function and the parameter σ is the waveform's width. Hence, it is assumed that $i_n^+(t)=w_k(t)$, for any $n=1\ldots N$.

The $k=0$ function (Fig. 2) is a Gaussian pulse, $k=1$ gives a monocycle and $k=2$ a doublet. All the functions of parameter σ are up-bounded by a zeroth order Gaussian pulse of larger parameter: $exp(-t^2/4\sigma^2)$.

The Fourier transform of (4) is

$$W_k(\omega)=\frac{(-j)^k(\sqrt{2}\sigma)^k}{\sqrt{2^k k!}}\omega^k\exp\left(-\frac{\omega^2\sigma^2}{2}\right) \tag{5}$$

and its spectrum peaks at $\omega_k=\sqrt{k}/\sigma$. The HR functions exhibit a compact support in both time and frequency domains and can be generated by a cascade of differentiation modules. Such functions are generally accepted as typical input signals in real transmitters (see for instance [16], [26]), and more complex finite-support waveforms can be synthesized as a superposition of HR functions [18], [27]. A discussion on this issue is presented in Section V.

The space-time dispersive effect of the radiating elements is taken into account by means of the following simple mathematical model of the antenna's effective height, wherein the angular and time dependences are supposed decoupled such as

$$\boldsymbol{h}^t(\hat{\boldsymbol{r}},\tau)=\boldsymbol{g}(\hat{\boldsymbol{r}})\delta^{(q)}(\tau-\tau_q) \tag{6}$$

where τ_q is a time delay and the operator $\delta^{(q)}$, as already discussed in [16] and in [18], produces the qth derivative of the input signals. It is worth noticing (see the review in [28] for an extensive gallery of the transient response of antennas) that the case $q=1$ (ideal differentiator) is a good model for optimal UWB antennas (TEM horn, IRA), the case $q=2$ represents the response of a small dipole [24] and, finally, $q=3$ close resembles the impulse response of moderately large-band antennas such as a diamond dipole [29] and the Achimedean spiral. This representation could be also extended to more complex impulse responses by a linear combination of derivative operators. Nevertheless, the only canonical cases described by (6) will be here

considered, while some more realistic models will be discussed in Section V.

Thanks to the distributive property of the differentiator operator with respect to the convolution (e.g., $\delta^{(q)} * \mathcal{F} \Rightarrow \sum \delta^{(q)} * w_k(t)$) and to the definition of HR functions, the overall field radiated by the circular array sourced by above input stimuli may be rewritten as

$$\boldsymbol{E}^A(\boldsymbol{r},t) = -\frac{\eta_0}{4\pi c}\frac{\boldsymbol{g}(\hat{\boldsymbol{r}})}{r}A_{k,q}\sum_{n=1}^{N} w_{k+q}\left(t-\frac{r}{c}+t_n(\hat{\boldsymbol{r}})-\tau_q\right) \tag{7}$$

where $A_{k,q} = \sqrt{2^q(k+q)!/k!}/(-\sqrt{2}\sigma)^q$ is a constant with $A_{k,0}=1$. Denoting with

$$\mathcal{F}_m(\hat{\boldsymbol{r}},\tau) = \sum_{n=1}^{N} w_m\left(\tau + t_n(\hat{\boldsymbol{r}}) - \tau_q\right)] \tag{8}$$

the mth order *Hermite-Rodriguez Array Factor*, which embodies both the input waveform order and the time-dispersive effect of the antennas ($m = k+q$), the array's total field will be finally proportional to

$$\boldsymbol{E}^A(\boldsymbol{r},t) \propto \frac{\boldsymbol{g}(\hat{\boldsymbol{r}})}{r}\mathcal{F}_m\left(\hat{\boldsymbol{r}}, t-\frac{r}{c}\right). \tag{9}$$

The array pattern can be globally characterized by the time duration, or *time resolution* of the main spot, and by its angular width or *angular resolution.*

The angular resolution is associated to an energy indicator, e.g., to an L_2 norm removing the time dependence in (9). Hence the *Energy Pattern* of the array, also accounting for the temporal-dispersive effect of the antennas and of the input signals may be defined as

$$\mathcal{E}_m(\hat{\boldsymbol{r}}) = \|\boldsymbol{g}\mathcal{F}_m\|_2^2(\hat{\boldsymbol{r}}) = |\boldsymbol{g}(\hat{\boldsymbol{r}})|^2\,\|\mathcal{F}_m\|_2^2(\hat{\boldsymbol{r}}) \tag{10}$$

where $\|\ldots\|_2$ is the L_2 norm with respect to time. The pattern multiplication principle still holds in the energy domain, so that it is possible to define a half-power beamwidth for the main spot in analogy to the frequency domain beamwidth. Calculation of $\|\mathcal{F}_m\|_2^2(\hat{\boldsymbol{r}})$ needs to be generally performed numerically, but interesting analytical formulas can be retrieved in the assumption of large number of elements as discussed in the Section III.

B. Time Resolution

The time resolution along the main beam is defined as the effective signal duration [24]

$$T = \frac{\left\|t\cdot\boldsymbol{E}^A(\boldsymbol{r}_0,t)\right\|_2}{\left\|\boldsymbol{E}^A(\boldsymbol{r}_0,t)\right\|_2}. \tag{11}$$

For a uniform array, T coincides with the duration of the mth HR function T_m, since $\boldsymbol{E}^A(\boldsymbol{r}_0,t) \propto N w_m(t)$ and it can be expressed (see Appendix) as

$$T_m = \sigma\sqrt{\frac{\Gamma\left(m-\frac{1}{2}\right)}{4\Gamma\left(m+\frac{1}{2}\right)}+1} \tag{12}$$

where Γ is the *Gamma* function. For example $T_m/\sigma = \{1.22, 1.08, 1.04, 1.03, 1.02\}$ for $m = 1$ to 5, while $T_m/\sigma \longrightarrow 1$ for further increasing m.

III. HR-Arrays With Many Elements

It is well known that the array factor $AF(\hat{\boldsymbol{r}},\omega)$ of a uniform circular array with a large number of elements, theoretically when N approaches infinity (continuous uniform current over a circle), can be expressed in the frequency domain [23] by means of the zeroth order Bessel function

$$AF(\hat{\boldsymbol{r}},\omega) \simeq NI(\omega)J_0\left(\frac{\omega}{c}\rho_0(\hat{\boldsymbol{r}})\right) \tag{13}$$

where $I(\omega)$ is the spectrum of the input signals and ρ_0 a trigonometric function independent on frequency

$$\rho_0(\hat{\boldsymbol{r}}) = R\sqrt{(\sin\theta\cos\phi-\sin\theta_0\cos\phi_0)^2+(\sin\theta\sin\phi-\sin\theta_0\sin\phi_0)^2} \tag{14}$$

where $\rho_0 = R\sin\theta$ for focusing along the vertical (z) axis ($\theta_0 = 0$) while $\rho_0 = 2R\sin((\phi-\phi_0)/2)$ when the main spot is formed on the horizontal array plane, e.g., for $\theta = \theta_0 = \pi/2$.

Taking the Fourier transform of (13), the HR array factor in case of many elements can be approximated by the integral representation

$$\mathcal{F}_m(\hat{\boldsymbol{r}},\tau) = \frac{1}{2\pi}N\int_{-\infty}^{+\infty} W_m(\omega)J_0\left(\frac{\omega}{c}\rho_0(\hat{\boldsymbol{r}})\right)e^{j\omega\tau}d\omega. \tag{15}$$

Above integral can be considered as a windowed (Gabor) Fourier Transform of the Bessel function and it is solved by using the expression in (5) for the HR function and the series definition [30] of the Bessel function $J_0(x)$. After some tedious but straightforward manipulations the expression in (15) is finally written as

$$\mathcal{F}_m(\rho_0,\tau) = N\sum_{p=0}^{\infty} B_{m,p}\left(\frac{\rho_0}{2c\sigma}\right)^{2p} w_{m+2p}(\tau)$$
$$B_{m,p} = \frac{1}{(p!)^2}\sqrt{\frac{(m+2p)!}{m!}}. \tag{16}$$

In particular, for beam focusing along the array plane ($\rho_0 = 2R\sin((\phi-\phi_0)/2)$), the above expression becomes

$$\mathcal{F}_m(\rho_0,\tau) = N\sum_{p=0}^{\infty} B_{m,p}\left(\frac{R}{c\sigma}\right)^{2p}\sin^{2p}\left(\frac{\phi-\phi_0}{2}\right)w_{m+2p}(\tau). \tag{17}$$

A. Pattern Formation

It is worth noting that along the main beam ($\phi = \phi_0$) the 0th term in (17) is the only surviving one and hence $\mathcal{F}_m(\rho_0,\tau) = N w_m(\tau)$, as expected. At other directions, the radiated field is given by the superposition of infinite high-order HR waveforms whose amplitude is angularly modulated by the $\sin^{2p}((\phi-\phi_0)/2)$ factor (or by $\sin^{2p}\theta$ for focusing on the vertical direction). Such waveforms are therefore as more

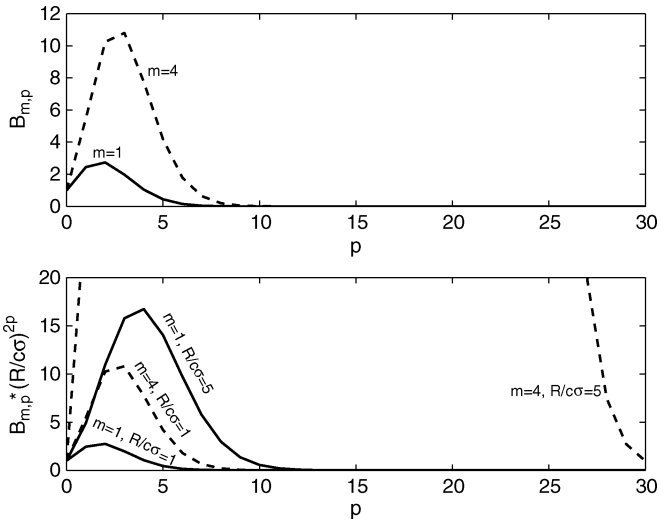

Fig. 3. Excitation coefficients $B_{m,p}$ and $(R/c\sigma)^{2p}B_{m,p}$ of the HR waves in (17) for some choices of the order m and of size R with respect to the input signal duration.

weighted as the observation direction departs from the main beam. However, the number of emitted waves is practically limited since the excitation coefficients $\{B_{m,p}(R/c\sigma)^{2p}\}_p$ exhibit a low-pass behavior as shown, for example in Fig. 3. The span of the practically excited waves enlarges along with the size of the array (with respect to the input pulse duration, e.g., $R/c\sigma$), and with the array order m. In other words, only a limited set, among the infinite HR waves emitted from the array, will contribute to the propagation. For instance, in case $R = c\sigma$ and ideal antennas ($q = 1$) sourced with Gaussian pulses ($k = 0$), the practically excited HR functions are less than 10.

Far from the main beam, the w_{m+2p} waveforms interfere and, as sketched in Fig. 4(a), the internal out-of-phase oscillations of the multiplicity of signals tend to mutually cancel leaving a couplet of external residual waists. The resulting angle-time pattern exhibits a typical "X"-like shape, whose vertex gives the main spot and the external fringes have the meanings of the side-lobes. The sequence of $\mathcal{F}_m$ images in the example of Fig. 4(b) provides evidence of the above discussed cancellation of internal oscillations and of the finite number of excited HR waves. This kind of pattern is typical of uniform current distributions on circles, in the context of the "X"-waves theory [22]. These concepts are further enlighten in the example Section.

B. Angular Resolution

A significant expression for the energy pattern in (10) is now found by starting from (15) and calculating $\|\mathcal{F}_m\|_2^2$ in the frequency domain through the Parseval theorem and using the spectrum in (5):

$$\frac{\mathcal{E}_m(\hat{\boldsymbol{r}})}{|\boldsymbol{g}(\hat{\boldsymbol{r}})|^2} = \frac{N^2}{(2\pi)^2}\frac{\sigma^{2m}}{m!}\int \omega^{2m} J_0^2\left(\frac{\omega}{c}\rho_0(\hat{\boldsymbol{r}})\right) e^{-\omega^2\sigma^2} d\omega. \quad (18)$$

The above integral has an exact solution in terms of the *Generalized Hypergeometric Function* ${}_2F_2$ [31], as described

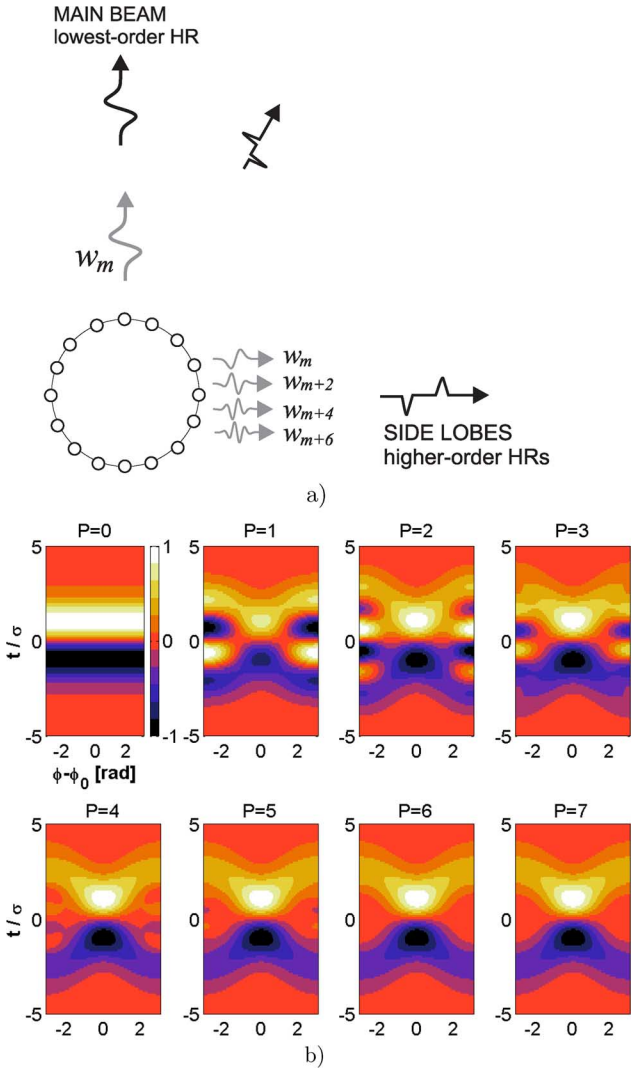

Fig. 4. Formation of the TD radiation pattern of an Hermite-Rodriguez array timed to focus along the horizontal plane. a) Sketch of the far field waveforms, $w_m(t)$, along the main beam and far from it (superposition of higher order HRs $w_{m+2q}(t)$). b) Example of "X"-shaped pattern formation ($m = 1$, $R = c\sigma$) for increasing truncation $p = 0 \ldots P$ of the series in (16).

in the Appendix. After some mathematical manipulation, (18) becomes

$$\frac{\mathcal{E}_m(\hat{\boldsymbol{r}})}{|\boldsymbol{g}(\hat{\boldsymbol{r}})|^2} = \frac{1}{(2\pi)^2}\frac{N^2}{2\sigma m!}\Gamma\left(\frac{2m+1}{2}\right) \times {}_2F_2\left(\frac{1}{2}, \frac{2m+1}{2}; 1, 1; -u^2(\hat{\boldsymbol{r}})\right) \quad (19)$$

having introduced the auxiliary variable $u(\hat{\boldsymbol{r}}) = \rho_0(\hat{\boldsymbol{r}})/(c\sigma)$. The peak value of (19), corresponding to $\hat{\boldsymbol{r}} = \hat{\boldsymbol{r}}_0$, appears for $u = 0$ and, accordingly, ${}_2F_2((1/2), (2m+1/2); 1, 1; 0) = 1$.

Fig. 5 shows the plot of the normalized $\mathcal{E}_m(\hat{\boldsymbol{r}})/|\boldsymbol{g}(\hat{\boldsymbol{r}})|^2$ angular energy for some orders m, versus the auxiliary variable u. The width of the main-lobe reduces for increasing m and the first side-lobe appears for $m \geq 3$ while further lobes may be recognized for $m = 10$.

The angular resolution of the mth HR array factor, e.g., the angle wherein the energy pattern $\|\mathcal{F}_m\|_2^2$ is not less than half the

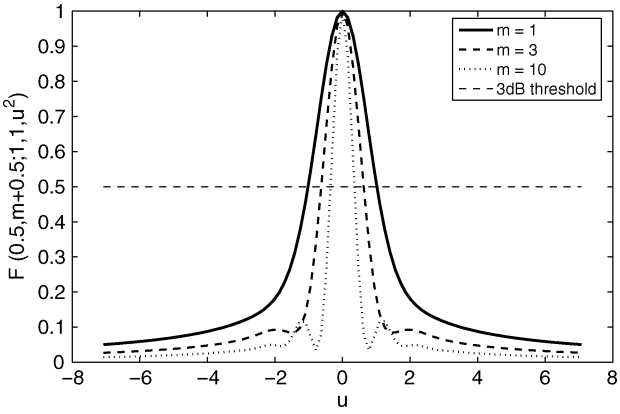

Fig. 5. Normalized energy pattern of the HR array $\mathcal{E}_m(\hat{\boldsymbol{r}})/|\boldsymbol{g}(\hat{\boldsymbol{r}})|^2$ versus the auxiliary variable $u = \rho_0/cT$ for some orders m. The horizontal line tags the -3 dB amplitude for the calculation of the u_m values, and hence of the angular resolution.

TABLE I
HALF-POWER VALUES FOR THE HYPERGEOMETRIC SERIES

m	u_m	m	u_m
0	2.33	4	0.57
1	1.06	5	0.51
2	0.79	6	0.48
3	0.69	7	0.45

peak value, is calculated by enforcing

$$ {}_2F_2\left(\frac{1}{2}, \frac{2m+1}{2}; 1, 1; -u_m^2\right) = \frac{1}{2}. \tag{20}$$

The first values of u_m are given in Table I.

The angular resolution of the array factor is finally retrieved for array focusing along the vertical and the horizontal planes. In the first case $u = (R/c\sigma)\sin\theta$ and the visible space is limited by

$$|u| < \frac{R}{c\sigma} \tag{21}$$

which is accordingly affected by the radius of the array and by the time duration of the pulse. The angular resolution, Θ_m, is obtained by enforcing $u = u_m$ so that

$$\Theta_m = 2\sin^{-1}\left(\frac{c\sigma}{R}u_m\right) \tag{22}$$

For directive arrays this expression simplifies as follows:

$$\Theta_m \simeq 2\frac{c\sigma}{R}u_m. \tag{23}$$

Having fixed the array radius, the angular resolution can be therefore improved by increasing the order of the input signal (or of the antenna), at expense of the formation of energy side-lobes, as well as by reducing the input signal duration.

A similar expression

$$\Phi_m \simeq 2\frac{c\sigma}{R}u_m \tag{24}$$

can be found for an array focusing on the horizontal plane ($|u| < (2R/c\sigma)$) along a direction $\phi_0 = 2\ell\pi/N$, where ℓ is an integer number.

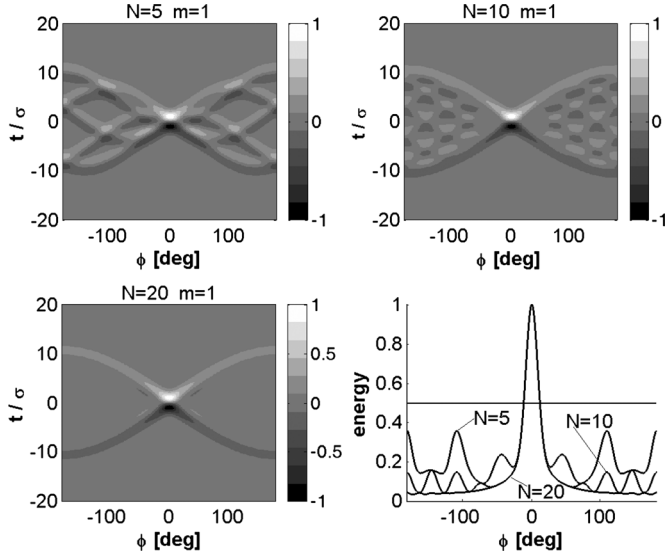

Fig. 6. TD array factor $\mathcal{F}_1(\hat{\boldsymbol{r}}, \tau)$ and angular energy on the horizontal plane $\theta = \pi/2$ timed to focus at $(\hat{\boldsymbol{r}}_0 = \widehat{\boldsymbol{x}})$ for electric and geometric parameters: $\sigma = 0.1$ ns, array radius $R = 5c\sigma$ and increasing number of array elements $N = \{5, 10, 20\}$.

It is worth noticing that expression in (23) and (24) generalizes those in [23] to higher order pulses and multiple differentiating antennas.

IV. NUMERICAL EXAMPLES

Space-time-patterns and energy diagrams are here shown with respect to some choices of the electrical and geometrical features of the HR array. An elementary pattern synthesis is also illustrated.

In all the given examples only the signal distortion effect of the antennas is considered while, for generality, the angular spreading function $\boldsymbol{g}(\hat{\boldsymbol{r}})$ is dropped (which means to consider antennas with isotropic radiation, at least over the observation plane).

A. Radiation Versus Number of Antennas

Fig. 6–8 shows the $\mathcal{F}_1(\hat{\boldsymbol{r}}, \tau)$ for the case of input pulses with Gaussian width $\sigma = 0.1ns$ and array radius $R = 5c\sigma$, concerning spot focusing along the horizontal plane $(\hat{\boldsymbol{r}}_0 = \hat{x})$ and along the vertical plane $(\hat{\boldsymbol{r}}_0 = \hat{z})$, respectively. The diagrams are specified for increasing numbers of elements $N = \{5, 10, 20\}$. The resulting space-time functions may represent the radiation from ideal antennas sourced by Gaussian pulses.

The presence of side partial interferences among a subset of emitters is clearly visible. The interference fringes, outside the main spot are quite different for the case of vertical and horizontal focusing. On the vertical plane, the phenomenology is rather similar to that of a linear array and side "interference rails" appears, due to the radiation of each emitters [32]. On the horizontal plane instead, the interference pattern is more complicated and N true distinct multiple side spots are visible at the left-side and at the right-side of the main spot. These are produced by the mutual interference originating by couplets of

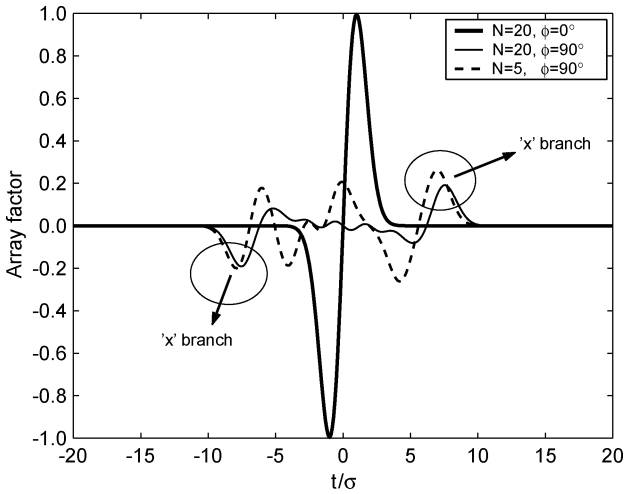

Fig. 7. Some cuts of $\mathcal{F}_1(\cdot,\tau)$ from the 2D representation in Fig. 6 for different numbers of elements and observation directions. Functions are normalized with respect to the maximum amplitude. The branches of the "X" shape are clearly visible.

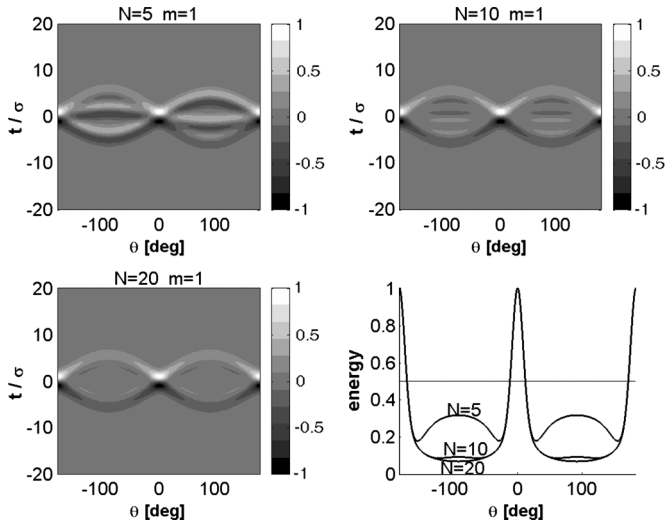

Fig. 8. TD array factor $\mathcal{F}_1(\hat{\boldsymbol{r}},\tau)$ on the vertical plane $\phi = 0$ timed to focus at $(\hat{\boldsymbol{r}}_0 = \hat{\boldsymbol{z}})$ for electric and geometric parameters: $\sigma = 0.1$ ns, array radius $R = 5c\sigma$ and increasing number of array elements $N = \{5, 10, 20\}$.

emitters placed at different distance from the axis $(\hat{y})$ orthogonal to the focusing direction $(\hat{x})$ so that their delays are synchronized at a particular direction. However, in both the configurations, as the density of elements increases, the positive pulse of a spot cancels the negative pulse of the adjacent one, only leaving the most external fringes (Fig. 7). The resulting pattern is the "X" shape, already discussed in the previous Section from a different point of view. The energy diagrams reveal that, while the angular resolution remains unchanged with respect to the increase in the number of elements, the side spots become instead sensibly lower. It is worth mentioning that extensive numerical simulations demonstrate that the representations (16) and (17) are able to reproduce the whole "X" phenomenology when just $N > 20 \sim 30$ with a weak dependence on the array size, also for radius $R = (10 \sim 50)c\sigma$. Such approximations are therefore valid even when the inter-antenna distance (element density) is not particular small (in terms of the waveform duration).

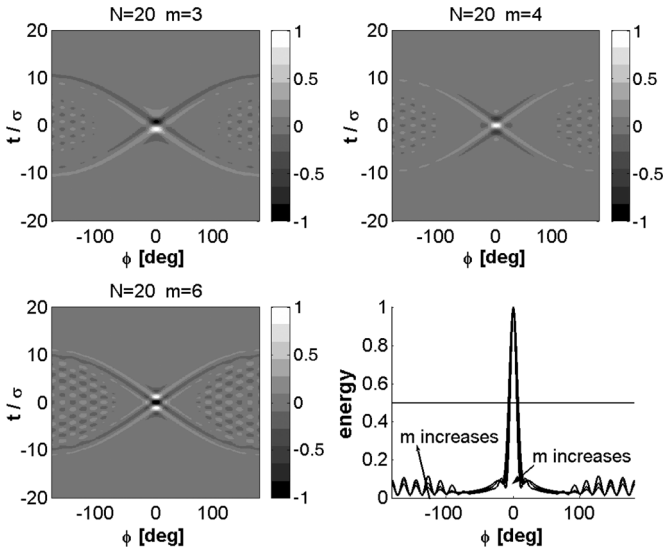

Fig. 9. TD array factor $\mathcal{F}_m(\hat{\boldsymbol{r}},\tau)$ and angular energy on the horizontal plane $\phi = 0$ timed to focus at $(\hat{\boldsymbol{r}}_0 = \hat{\boldsymbol{x}})$ for three different order $m = \{3, 4, 6\}$. Other parameters as in the previous examples.

B. Radiation vs. Array Order

The previous numerical experiments are now repeated for higher order array factors $\mathcal{F}_m(\hat{\boldsymbol{r}},\tau)$ with $m = \{3,4,6\}$ which may represent several combinations of antenna types and input signal's orders. Just for instance, the case $m = 3$ represents the radiation of broadband dipoles (diamond-like, $q = 3$) sourced by Gaussian pulses ($k = 0$), as well as small dipoles ($q = 2$) sourced by monocycles ($k = 1$). The case with $m = 4$ may reproduce the radiation of broadband dipoles ($q = 3$) with differentiated Gaussian input signals ($k = 1$). Results are given in Fig. 9 where multiple time oscillations appear along the main spot with increasing order of the HR functions. When comparing Fig. 9 with the $m = 1$ case in Fig. 6, it is possible to note a narrowing in the main spot and a more "pixelated" pattern of side spots as also apparent in the energy diagram. The corresponding angular resolutions are $\Phi_m = (2/5)u_m = \{24°, 16°, 13°, 11°\}$ for $m = \{1, 3, 4, 6\}$.

C. Example of Synthesis

Equations (10) and (22) or (23) help to choose the values of driving Gaussian pulses' parameter σ and of the array radius to achieve the desired temporal and angular resolution, for the particular pulses' order and antenna family. For instance, in case of focusing over the array plane, the array size R is related to the spot's resolution by the equation

$$R = \left(\frac{2cu_m}{\alpha_m}\right)\frac{T_m}{\Phi_m} \tag{25}$$

where $\alpha_m = T_m/\sigma$ as derived from (10).

Just for example, consider the synthesis of a narrow beam with required resolution $T = T_m = 1$ ns and $\Phi = \Phi_m = 5°$. In case of an array of ideal UWB antennas $(q = 1)$ sourced by Gaussian pulses $(k = 0)$ the needed array radius from (25) is $R(m = 1) = 5.95$ m, while a rather smaller radius is required in case ultra wideband dipoles $(q = 3)$ and input monocycles $(k = 1)$ are used, e.g., $R(m = 4) = 3.20$ m. It is interesting

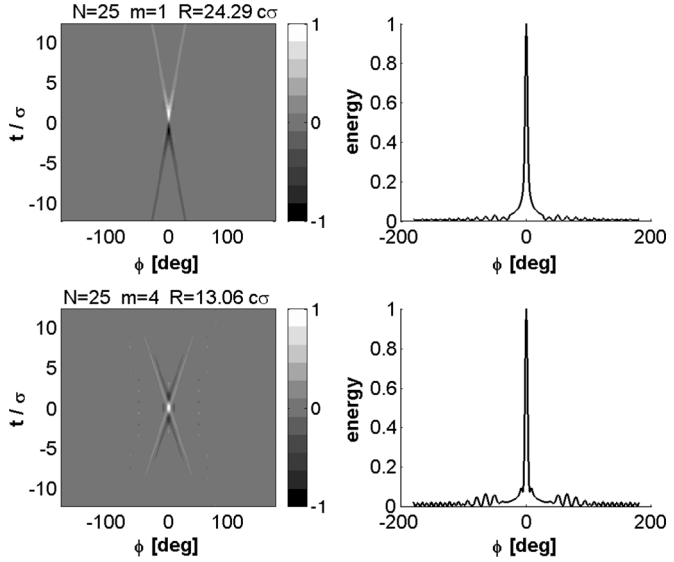

Fig. 10. HR array factors and angular energies for two choices of antennas family and input signal waveforms such to give, in both the cases, the same temporal- and angular-resolution $(T, \Phi) = (5\ \mathrm{ns}, 5^\circ)$. Upper row: $m = 1$ with a required radius $R = 5.95\ \mathrm{m}$. Lower row: $m = 4$ with a required radius $R = 3.20\ \mathrm{m}$.

to note that these sizes are in full agreement with those found in [32] for the case of linear arrays with the same resolution. The angle-time and energy patterns for the above examples are displayed in Fig. 10 for the case of $N = 25$ elements. It can be observed that the highest order HR array factor exhibits a more localized "X" pattern than the $\mathcal{F}_1$ case.

V. Extension to Real Arrays

Real antennas and real input signals may differ from the canonical models given above. For instance the input signal could be a differently synthesized waveform, or the antennas' impulse response could be not symmetric or decay less regular than a single HR function. Nevertheless the presented formulation can be still useful to manage the dominant behavior of real systems. At this purpose the complexity of the real word is parametrized again by the help of the HR functions which are a useful tool to represent compact-support signals [25]. In particular, both the input current and the time-dependence of the antennas' impulse response are represented as a finite superposition of HR families having, for generality, different parameters σ, μ, respectively

$$i(t) = \sum_{k=0}^{K} i_k w_{\sigma,k}(t) \tag{26}$$

$$\boldsymbol{h}^t(\hat{\boldsymbol{r}}, \tau) = \boldsymbol{g}(\hat{\boldsymbol{r}}) \sum_{q=1}^{Q} h_q w_{\mu,q}(\tau - \tau_\ell) \tag{27}$$

where $\{i_k\}$ and $\{h_q\}$ are constant coefficients and the HF functions are defined as in (4) with proper Gaussian width as indicated in the subscript. t_ℓ is a time delay assumed to be identical for all the functions. The representation in (27) can be considered as a generalization of the ideal model in (6) wherein the qth derivative is replaced by a finite realization which broaden the input signal. The total field in (1) is therefore written as a triple summation

$$\boldsymbol{E}^A(\boldsymbol{r}, t) = -\frac{\eta_0}{4\pi c} \frac{\boldsymbol{g}(\hat{\boldsymbol{r}})}{r} \tag{28}$$

$$\sum_{q=1}^{Q} \sum_{n=1}^{N} \sum_{k=0}^{K} h_q i_k \left[w_{\sigma,k}() * w_{\mu,q}() \right] \left(t - \frac{r}{c} + t_n(\hat{\boldsymbol{r}}) \right) \tag{29}$$

The convolution between two HR functions of different widths is still an HR function [25] having order equal to the sum of the two orders and width, α, given by the average quadratic summation of the two widths, e.g.,

$$w_{\sigma,k}(t) * w_{\mu,q}(t) = \frac{\mu^q \sigma^k}{\sqrt{(\sigma^2 + \mu^2)^{q+k}}} \sqrt{\frac{(q+k)!}{q!k!}} w_{\alpha,q+k}(t) \tag{30}$$

with $\alpha = \sqrt{\sigma^2 + \mu^2}$. Denoting with $A_{k,q} = h_q i_k (\mu^q \sigma^k / \sqrt{(\sigma^2 + \mu^2)^{q+k}}) \sqrt{(q+k)!/q!k!}$, then the total field becomes

$$\boldsymbol{E}^A(\boldsymbol{r}, t) = -\frac{\eta_0}{4\pi c} \frac{\boldsymbol{g}(\hat{\boldsymbol{r}})}{r} \sum_{q=1}^{Q} \sum_{k=0}^{K} A_{k,q} \mathcal{F}_{\alpha,q+k} \left(\hat{\boldsymbol{r}}, t - \frac{r}{c} - \tau_\ell \right) \tag{31}$$

where $\mathcal{F}_{\alpha,q+k}(\hat{\boldsymbol{r}}, t)$ is the array factor as defined in (8) for an ideal HR array with input signals of width α. The real array may be therefore interpreted as the superposition of $Q \times K$ $(q - k)$th order HR arrays with weights $\{A_{k,q}\}$. Along the main spot the signals are all synchronized, $\mathcal{F}_{q+k} \propto N w_{\alpha,q+k}$, and hence by reordering the terms, the radiated field is the superposition of HR functions of same width and different orders, e.g., $\boldsymbol{E}^A(\boldsymbol{r}_0, t) \propto \sum_{m=0}^{Q+K} A_m w_{\alpha,m}$. The strongest coefficient $A_{\bar{m}}$ identifies the *dominant* HR contributing function $w_{\alpha,\bar{m}}$ to the radiation, in the sense of a weighted quadratic norm since $\int_{-\infty}^{+\infty} |\boldsymbol{E}^A(\boldsymbol{r}_0, t)|^2 e^{t^2/2\alpha} dt \propto \sum_m |A_m|^2$ [25]. The corresponding $\mathcal{F}_{\alpha,\bar{m}}$ terms can be considered as the dominant HR array factor whose phenomenology and resolutions gives a first-order indication of the whole array features. The macroscopic difference with respect to the ideal case is that the width of the transmitted signal will be now enlarged $(\sigma \to \sqrt{\sigma^2 + \mu^2})$ by the presence of the antennas and hence the time and angular resolutions are expected to be degraded.

It is worth finally recalling that all the given representations have been derived neglecting the antenna coupling. The formal analysis of the circular array coupling is beyond the scope of this paper but recalling a previous study of the authors [32] about the coupling in pulsed linear array, it is expected that the coupling should be a second-order phenomenon which is going to affect only slightly the shape of the main spot without sensible modification in its overall characteristics. Moreover, the inter-element distance may not be mandatory small to achieve a high resolution and the characteristic "X" waveform, and it is known that the coupling effect can be however greatly reduced by using input signals with small duration in comparison with the inter-antenna spacing (normalized by the light speed). The given results and guidelines are therefore considered of general applicability in the first step of real array design.

VI. Conclusion

The Hermite-Rodriguez formalism offers a compact representation of UWB arrays with high-order excitation also accounting, in a uniform way, for the distorting effect introduced by the antennas. The main results are now summarized.

i) A circular array with many UWB antennas, sourced by high-order Gaussian pulses, produces a time-varying pattern which is the superposition of a practical finite set of Hermite-Rodriguez waveforms, angularly weighted, giving an "X"-shaped space-time pattern;
ii) Hence the radiation is practically localized in angle, time and even in waveform domains. The energy pattern is a ${}_2F_2$ generalized Hypergeometric function;
iii) The time resolution is dependent on both the input waveform's order and duration and on the distortion's order of the antennas. However the time resolution tends to saturate to the Gaussian parameter σ as $m > 4$;
iv) The angular resolution improves (Θ_m, Φ_m reduce) by increasing the order of the HR array;
v) The space-time localization globally improves with the increase of the array size;
vi) The HR array has still some meaning in case of realistic systems with more complicated dispersive behavior since it gives information about the dominant contribute to the radiation;
vii) The angle-time resolution of a real array is expected to be worse than in the case of a canonical HR array of same geometry.

The presented simple mathematical dissertation permits not only to give some physical insight to the complex time-domain radiation mechanism, but also provides a first tool for an elementary array synthesis wherein both the angular- and the time-resolution are subjected to constraints. The array resolution and the strength of side spot may be controlled not only by the array size and by the number of elements, but also by acting on the order and on the duration of input pulses and by selecting the proper distorting effect of the antennas.

Appendix

A. Details About the Calculation of T_m in (12)

The effective signal duration [24] of the mth HR function is formally defined as

$$T_m = \frac{\|t \cdot w_m(t)\|_2}{\|w_m(t)\|_2}. \tag{32}$$

It is now convenient to express the HF functions in terms of the Hermite polynomials H_m, e.g., $w_m(t) = (1/\sqrt{2^m m!})H_m(t/\lambda)(1/\sqrt{\pi}\lambda)\exp[-(t^2/\lambda^2)]$, with the scale factor $\lambda = \sqrt{2}\sigma$. By using the definition $H_2(t) = 2(2t^2 - 1)$ and by some mathematical manipulation, the numerator in (32) is rewritten as in (33), shown at the bottom of the page.

The denominator is instead

$$\|w_m(t)\|_2 = \sqrt{\int \frac{1}{2^m m!\pi\lambda^2} H_m^2\left(\frac{t}{\lambda}\right)\exp\left[-\frac{2t^2}{\lambda^2}\right]dt}. \tag{34}$$

The above integrals are of the types [33]

$$\int \exp[-2x^2]H_k(x)H_m(x)H_n(x)dx = \frac{1}{\pi}2^{\frac{1}{2}(m+n+k-1)}\Gamma(s-k)\Gamma(s-m)\Gamma(s-n)$$

$$\int \exp[-2x^2]H_m(x)H_n(x)dx = (-1)^{\lfloor\frac{m}{2}\rfloor+\lfloor\frac{n}{2}\rfloor}2^{\frac{m+n+1}{2}}\Gamma\left(\frac{m+n+1}{2}\right)$$

with $2s = k + m + n + 1$, and hence

$$\|t \cdot w_m(t)\|_2 = \sqrt{\frac{\sqrt{2}\sigma}{4m!\pi^2}\left[\sqrt{2}\Gamma\left(m-\frac{1}{2}\right)\Gamma^2\left(\frac{3}{2}\right) + \frac{2\pi}{\sqrt{2}}\Gamma\left(m+\frac{1}{2}\right)\right]} \tag{35}$$

$$\|w_m(t)\|_2 = \sqrt{\frac{1}{2m!\pi\sigma}\Gamma\left(m+\frac{1}{2}\right)}. \tag{36}$$

Finally

$$T_m = \sigma\sqrt{\frac{\Gamma\left(m-\frac{1}{2}\right)\Gamma^2\left(\frac{3}{2}\right)}{\pi\Gamma\left(m+\frac{1}{2}\right)} + 1}. \tag{37}$$

B. Details About the Calculation of the Energy Pattern in (18)

The integral in (18) is of the type

$$\int x^{\lambda-1}\exp(-\alpha x^2)J_a(\beta x)J_b(\beta x)dx = 2^{-a-b-1}\alpha^{-\frac{1}{2}(a+\lambda+b)}\beta^{v+u}\frac{\Gamma\left(\frac{\lambda+a+b}{2}\right)}{\Gamma(a+1)\Gamma(b+1)} \times {}_3F_3\left(\frac{a+b+1}{2}, \frac{a+b+2}{2}, \frac{a+b+\lambda}{2}; a+1, b+1, a+b+1; -\frac{\beta^2}{\alpha}\right) \tag{38}$$

where ${}_3F_3$ is the Hypergeometric Function [30], [31], [34], defined as

$${}_pF_q(a_1,\ldots,a_p;b_1,\ldots,b_q;z) = \sum_{k=0}^{\infty}\frac{(a_1)_k(a_2)_k\cdots(a_p)_k}{(b_1)_k(b_2)_k\cdots(b_q)_k}\frac{z^k}{k!}. \tag{39}$$

$$\|t \cdot w_m(t)\|_2 = \sqrt{\frac{\lambda}{2^{m+2}m!\pi}\int H_2(t)H_m^2(t)\exp[-2t^2]dt + \frac{\lambda}{2^{m+1}m!\pi}\int H_m^2(t)\exp[-2t^2]dt}. \tag{33}$$

The term $(x)_n$ is the Pochhammer operator

$$(x)_n = x(x+1)(x+2)\cdots(x+n-1) = \frac{\Gamma(x+n)}{\Gamma(x)}. \quad (40)$$

After substitution $x = \omega$, $\lambda - 1 = 2m$, $\alpha = \sigma^2$, $\beta = \rho_0/c$, $a = b = 0$, $u = \rho_0/c\sigma$ and the simplifications ${}_3F_3((1/2), 1, (2m+1)/2; 1, 1, 1; -u^2) = {}_2F_2((1/2), (2m+1)/2; 1, 1; -u^2)$, the (19) is obtained. The convergence of the function ${}_2F_2$ can be discussed by applying the definition in (39) and hence

$$\begin{aligned} &{}_2F_2\left(\frac{1}{2}, \frac{2m+1}{2}; 1, 1; -u^2\right) \\ &= \sum_{k=0}^{\infty} \frac{\left(\frac{1}{2}\right)_k \left(\frac{2m+1}{2}\right)_k}{(1)_k (1)_k} \frac{(-1)^k}{k!} u^{2k} \\ &= \frac{1}{\sqrt{\pi}} \sum_{k=0}^{\infty} \Gamma\left(\frac{1}{2}+k\right) \Gamma\left(\frac{2m+1}{2}+k\right) \frac{(-1)^k}{(k!)^3} u^{2k} \quad (41) \end{aligned}$$

where the following identities have been used:

$$\left(\frac{1}{2}\right)_k = \frac{\Gamma\left(\frac{1}{2}+k\right)}{\Gamma\left(\frac{1}{2}\right)} = \frac{\Gamma\left(\frac{1}{2}+k\right)}{\sqrt{\pi}}$$

$$\left(\frac{2m+1}{2}\right)_k = \frac{\Gamma\left(\frac{2m+1}{2}+k\right)}{\Gamma\left(\frac{2m+1}{2}\right)}.$$

The series in (41) is convergent according to the Leibniz rule since the terms have alternate sign and it is easy to show that they are uniformly decreasing after a given $k = K$ and finally each term goes to zero as $k \to \infty$.

ACKNOWLEDGMENT

The authors wish to thank Prof. R. Ziolkowski for having suggested interesting papers on X-waves.

REFERENCES

[1] C. E. Baum, "Transient arrays," in *Proc. Ultra-Wideband, Short-Pulse Electromagnetics 3*, C. E. Baum, Ed. *et al.* New York: Plenum Press, 1997, pp. 129–138.

[2] E. L. Mokole, "Behavior of ultrawideband-radar array antennas," in *Proc. IEEE Int. Symp. on Phased Array Systems and Technology*, 1996, pp. 113–118.

[3] F. Anderson, W. Christensen, L. Fullerton, and B. Kortegaard, "Ultrawideband beamforming in sparse arrays," *Proc. Inst. Elect. Eng.*, vol. 138, no. 4, pt. H, pp. 342–346, 1991.

[4] K. Siwiak and D. McKeown, *Ultra-Wideband Radio Technology*. New York: Wiley, 2004.

[5] M. Ghavami, L. B. Michael, and R. Kohno, *Ultra Wideband: Signals and Systems in Communication Engineering*. Chichester, U.K.: Wiley, 2004, pp. 31–37.

[6] M. G. M. Hussain, "Principles of space-time array processing for ultrawide-band impulse radar and radio communications," *IEEE Trans. Veh. Technol.*, vol. 51, no. 3, pp. 393–403, 2002.

[7] M. Malek and M. Hussain, "Antenna patterns of nonsinusoidal waves with the time variation of a Gaussian pulse: Part I," *IEEE Trans. Antennas Propag.*, vol. 30, no. 4, pp. 504–512, Nov. 1989.

[8] M. Malek and M. Hussain, "Antenna patterns of nonsinusoidal waves with the time variation of a Gaussian pulse: Part II," *IEEE Trans. Antennas Propag.*, vol. 30, no. 4, pp. 513–522, Nov. 1989.

[9] A. Shlivinski and E. Heyman, "A unified kinematic theory of transient arrays," in *Ultra-Wideband Short-Pulse Electromagnetics 5*, P. D. Smith and S. R. Cloude, Eds. New York: Kluwer Academic/Plenum, 2000, pp. 327–334.

[10] G. Franceschetti, J. Tatoian, and G. Gibbs, "Timed arrays in a nutshell," *IEEE Trans. Antennas Propag.*, vol. 53, no. 12, pp. 4073–4082, 2005.

[11] W. Sorgel, C. Sturm, and W. Wiesbeck, "Impulse response of linear UWB antenna arrays and the application to beam steering," in *Proc. IEEE Int. Conf. on Ultra-Wideband*, 2005, pp. 275–280.

[12] Y. Kang and D. M. Pozar, "Optimization of pulse radiation from dipole arrays for maximum energy in a specified time interval," *IEEE Trans. Antennas. Propag.*, vol. 34, no. 12, pp. 1383–1390, 1986.

[13] J. L. Schwartz and B. D. Steinberg, "Ultrasparse, ultrawideband arrays," *IEEE Trans. Ultrason., Ferroelect., Freq. Control*, vol. 45, no. 2, pp. 376–393, Feb. 1998.

[14] L. B. Felsen and F. Capolino, "Time-domain Green's function for an infinite sequentially excited periodic line array of dipoles," *IEEE Trans. Antennas Propag.*, vol. 50, no. 1, pp. 31–41, Jan. 2002.

[15] F. Capolino and L. B. Felsen, "Time-domain Green's function for an infinite sequentially excited periodic planar array of dipoles," *IEEE Trans. Antennas Propag.*, vol. 51, no. 2, pp. 160–170, Feb. 2003.

[16] R. W. Ziolkowski, "Properties of electromagnetic beams generated by ultra-wide bandwidth pulse-driven arrays," *IEEE Trans. Antennas Propag.*, vol. 40, no. 8, pp. 888–905, 1992.

[17] J. E. Hernandez, R. W. Ziolkowski, and S. R. Parker, "Synthesis of the driving functions of an array for propagating localized wave energy," *J. Acoust. Soc., Am.*, vol. 92, no. 1, pp. 550–562, Jul. 1992.

[18] M. Ciattaglia and G. Marrocco, "Time domain synthesis of pulsed arrays," *IEEE Trans. Antennas Propag.*, vol. 56, no. 7, pp. 1928–1938, Jul. 2008.

[19] H. Arslan, Z. N. Chen, and M. G. Di Benedetto, *Ultra Wideband Wireless Communication*. Hoboken, NJ: Wiley-Interscience, 2006, ch. 3.

[20] C. Gentile, A. J. Braga, and A. Kik, "A comprehensive evaluation of joint range and angle estimation in ultra-wideband location systems for indoors," in *Proc. IEEE Int. Conf. on Commun.*, May 2008, pp. 4219–4225.

[21] D. De Vries, L. Horchens, and P. Grond, "Extraction of 3D information from circular array measurements for auralization with wave field synthesis," *J. Appl. Signal Process.*, vol. 2007, no. 1, pp. 190–200, 2007.

[22] , H. E. Hernandez-Figueroa, M. Zamboni-Rached, and E. Recami, Eds., *Localized Waves*. Hoboken, NJ: Wiley, 2008.

[23] M. G. M. Hussain, M. M. Al-Halabi, and A. A. Omar, "Antenna patterns of nonsinusoidal waves with the time variation of a Gaussian pulse: Part III," *IEEE Trans. Antennas Propag.*, vol. 31, no. 1, pp. 34–47, Feb. 1989.

[24] A. Shlivinski, E. Heyman, and R. Kastner, "Antenna characterization in the time domain," *IEEE Trans. Antennas Propag.*, vol. 45, no. 7, pp. 1140–1149, 1997.

[25] L. R. Lo Conte, R. Merletti, and G. V. Sandri, "Hermite expansion of compact support waveforms: Application to myoelectric signals," *IEEE Trans. Biomed. Eng.*, vol. 41, no. 12, pp. 1147–1159, Dec. 1994.

[26] M. Ghavami, L. B. Michael, and R. Kohno, *Ultra Wideband: Signals and Systems in Communication Engineering*. London, U.K.: Wiley, 2004, pp. 31–37.

[27] M. A. Yusoff, "Application of Hermite-Rodriguez functions to pulse shaping analog filter design," in *Proc. World Academy Sci., Eng. Technol.*, Dec. 2007, vol. 26, pp. 762–785.

[28] D. Ghosh, A. De, M. C. Taylor, T. Sarkar, M. C. Wicks, and E. Mokole, "Transmission and reception by ultra-wideband (UWB) antennas," *IEEE Antennas Propag. Mag.*, vol. 48, no. 5, pp. 67–99, Oct. 2006.

[29] H. Schantz, "Time domain array design," in *Ultra-Wideband Short-Pulse Electromagnetics 5*. New York: Kluwer Academic/Plenum Publisher, 2002, pp. 385–392.

[30] M. Abramowitz and I. A. Stegun, *Handbook of Mathematical Functions With Formulas, Graphs, and Mathematical Tables*. New York: Dover, 1964.

[31] E. W. Weisstein, *CRC Concise Encyclopedia of Mathematics*. Boca Raton, FL: Chapman & Hall/CRC Press, 1999, pp. 872–875.

[32] M. Ciattaglia and G. Marrocco, "Investigation on antenna coupling in time domain," *IEEE Trans. Antennas Propag.*, vol. 54, no. 3, pp. 835–843, March 2006.

[33] I. S. Gradshteyn and I. M. Ryzhik, *Table of Integrals, Series, and Products*, 7th ed. San Diego, CA: Elsevier, 2007.

[34] A. M. Mathai, *Generalized Hypergeometric Functions With Applications in Statistics and Physical Sciences*. Berlin: Springer-Verlag, 1973.

Gaetano Marrocco was born in Teramo, Italy, on August 29, 1969. He received the Laurea degree in electronic engineering and the Ph.D. degree in applied electromagnetics from University of L'Aquila, Italy, in 1994 and 1998, respectively.

He has been a Researcher at the University of Rome "Tor Vergata" since 1997 where he currently teaches antenna design and bioelectromagnetics. In summer 1994, he was at the University of Illinois at Urbana Champain as a Postdoctoral student. In autumn 1999, he was a Visiting Scientist at the Imperial College in London. His research is mainly directed to the modeling and design of broadband and ultrawideband antennas and arrays as well as of miniaturized antennas for RFID applications. He has been involved in several space, avionic, naval and vehicular programs of the European Space Agency, NATO, Italian Space Agency, and the Italian Navy. He holds two patents on broadband naval antennas and one patent on sensor RFID systems.

Prof. Marrocco currently serves as an Associate Editor of the IEEE ANTENNAS AND WIRELESS PROPAGATION LETTERS.

Giovanni Galletta received the Laurea degree in telecommunications engineering from the University of Rome "Tor Vergata" in 2008.

His main scientific interest concerns the design of antenna systems for telecommunications. He is currently employed at Terasystem SpA, Rome, Italy, where he works on IT Service Management.